Universidad de Cádiz

Dynamic Energy Management System of a Microgrid Cluster under Operational Intermittency

Horrillo Quintero, Pablo; García Triviño, Pablo; Carrasco González, David; Sarrias Mena, Raúl; García Vázquez, Carlos Andrés; Fernández Ramírez, Luis Miguel

Published in:
2025 5th International Conference on Electrical, Computer and Energy Technologies (ICECET)

DOI (link to publication from Publisher):
10.1109/ICECET63943.2025.11472139

Publication date:
2026

Document Version:
Camera ready

Citation for published version (IEEE):
P. Horrillo-Quintero, P. García-Triviño, D. Carrasco-González, R. Sarrias-Mena, C. A. García-Vázquez, and L. M. Fernández-Ramírez, "Dynamic Energy Management System of a Microgrid Cluster under Operational Intermittency," *2025 5th International Conference on Electrical, Computer and Energy Technologies (ICECET)*, pp. 1–6, Jul. 2025, doi: 10.1109/ICECET63943.2025.11472139.

979-8-3315-3559-9/25/$31.00 ©2025 IEEE

Dynamic Energy Management System of a Microgrid Cluster under Operational Intermittency

Pablo Horrillo-Quintero
SURET Research Group
Dept. Electrical Engineering
University of Cadiz
ETSI Algeciras, Spain
pablo.horrillo@uca.es

Pablo García-Triviño
SURET Research Group
Dept. Electrical Engineering
University of Cadiz
ETSI Algeciras, Spain
pablo.garcia@uca.es

David Carrasco-González
SURET Research Group
Dept. Electrical Engineering
University of Cádiz
ETSI Algeciras, Spain
david.carrasco@uca.es

Raúl Sarrias-Mena
SURET Research Group
Dept. Engineering in Automation, Elec.Comp.Arch & Net.
University of Cádiz
ETSI Algeciras, Spain
raul.sarrias@uca.es

Carlos A. García-Vázquez
SURET Research Group
Dept. Electrical Engineering
University of Cádiz
ETSI Algeciras, Spain
carlos.garcia@uca.es

Luis M. Fernández-Ramírez
SURET Research Group
Dept. Electrical Engineering
University of Cádiz
ETSI Algeciras, Spain
luis.fernandez@uca.es

***Abstract*— This paper presents a novel real-time dynamic energy management system for a microgrid cluster that includes renewable energy technologies, energy storage systems, and local demands. The energy management system operates as a tertiary controller, dynamically balancing power dispatch among microgrids by introducing the real-time available power concept. This work contributes by offering a flexible framework that coordinates both grid-forming and grid-following microgrids to optimize performance under variable renewable conditions. The proposed configuration comprises the integration of microgrids operating with grid-forming inverters and droop control method, alongside microgrids with grid-following inverter operating as an auxiliary microgrid. The proposed approach addresses the challenges of intermittency in renewable electrical technologies generation and demand variability, unlike traditional methods that assume ideal generation sources. It enables efficient, adaptive power distribution while ensuring that microgrids do not exceed their available capacities. The energy management system is validated through multiple time-domain simulations, by demonstrating its ability to maintain stability, resilience, and operational reliability in high-renewable energy technologies penetration scenarios.**

Keywords—Microgrid cluster, intermittency, dynamic, energy management system, grid-forming, grid-following.

I. INTRODUCTION

The urgent need to develop more sustainable and efficient energy systems is transforming how energy is generated and utilized. In recent years, microgrids (MGs) have emerged as a promising solution for the seamless integration of renewable energy technologies (RETs), energy storage systems (ESS), and consumer demand [1,2]. Taking the MG concept further, the interconnection of multiple MGs has given rise to the concept of the microgrid cluster (MGC). MGCs facilitate the coordinated management of multiple MGs, which is critical for ensuring seamless functionality, advanced control mechanisms, and effective resource distribution [3]. This arrangement enhances the system's resilience to dynamic changes, efficiently addressing variations in load demand, generation capacity, and operational requirements.

Power electronic converters are crucial for the stable integration of RETs and ESSs, mitigating low inertia challenges while enhancing stability and operational control in MGCs. Grid-forming (GFM) inverters play a key role in regulating frequency and voltage, allowing MGCs to operate independently from the main grid when needed [4]. Meanwhile, grid-following (GFL) inverters synchronize with the voltage and frequency at the coupling point to inject a controlled amount of power [5]. Together, these converters ensure flexibility, adaptability, and stability under dynamic conditions.

In the literature, research efforts have predominantly focused on addressing the study of MGC from a static optimization perspective. Reference [6] proposed an integrated multi-objective optimization strategy for a MGC with employed GFL inverters, considering operational costs. A grey wolf optimization algorithm was adopted to enhance MGC performance and ensure a reliable power supply. However, crucial aspects such as the dynamic behavior of the generation sources were not considered.

An approach to optimize energy management in a grid connected microgrid MGC was studied in [7]. The main goal

This work was partially supported by Ministerio de Ciencia e Innovación, Agencia Estatal de Investigación, FEDER, UE (Grant PID2021-123633OB-C32 supported by MCIN/AEI/10.13039/501100011033/FEDER, UE).

was to minimize operational costs and emissions through optimal utilization of the BESS. The slime mould algorithm was applied in combination with weighted sum and fuzzy decision-making methods to balance economic and environmental factors.

Reference [8] proposed a decentralized multilayer master-slave control strategy for managing direct current (DC) MGCs with multiple autonomous MGs. In this approach, an interlinking converter was used to connect two MGs and transmit power information, ensuring global power management. However, the generation units were modeled as ideal current sources, which may deviate from real dynamic behavior.

The control of RETs integrated into MGs using inverters under unbalanced load was analyzed in [9] based on the virtual conductance and negative sequence power. An isolated approach using GFM inverters was analyzed; nevertheless, the variability in generation was overlooked.

Addressing the intermittency of RETs and load variations in MGCs is increasingly critical as the share of variable energy sources grows in modern energy systems [10]. These fluctuations in both generation and demand present significant challenges to grid stability, particularly as the reliance on renewables continues to rise.

Current research on MGCs has predominantly focused on static optimization approaches. However, real-time control that accounts for the combination of GFM and GFL inverters has not been extensively studied. In particular, the real-time management of the operational intermittency of MGCs has not been deeply explored. Additionally, many studies [8,9,11,12] model RETs and ESS as ideal current sources connected to inverters, neglecting the dynamic behavior and variability inherent in these systems. Addressing this gap is crucial for improving MGC operation in real-world scenarios. Unlike previous studies that assume ideal generation sources, our approach accounts for real-time variations in renewable energy generation and demand.

This paper introduces a novel, real-time dynamic energy management system (EMS) designed to distribute power in a grid-connected MGC comprising RETs, ESSs, and local demands. The EMS functions as a tertiary controller, that dynamically balances power dispatch among microgrids, evaluating the real-time available power and demand within the MGC. A key feature of this approach is the integration of MGs operating in GFM with droop control, alongside MGs in GFL mode operating as auxiliary MGs.

The proposed EMS enables adaptive and efficient power distribution among MGs, addressing the operational intermittency of distributed generation and demand in real time. By incorporating the dynamics of RETs and ESSs, the proposed approach offers a robust and practical solution for improving the stability, resilience, and operational reliability of MGCs in real-world scenarios with high renewable energy penetration.

This paper is structured as follows: section II presents the MGC configuration, section III details the MGC control and the presented EMS, section IV analyzes and discusses the results and finally section V provides a conclusion of this work.

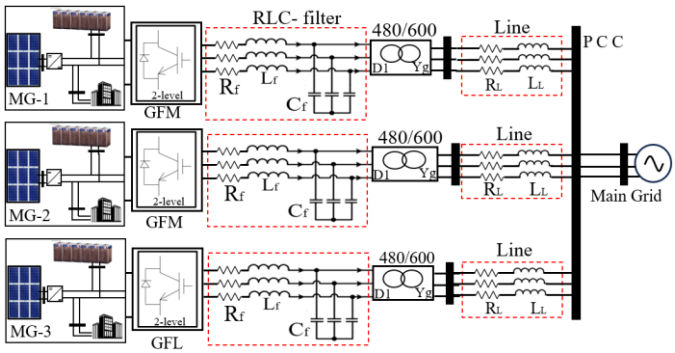

Fig. 1. MGC configuration.

II. Microgrid Cluster Configuration

In this section, the configuration of the grid-connected MGC under study is described. The MGC consists of three MGs, two of which are interconnected via GFM, while the third MG, operating as an auxiliary source, is connected through a GFL inverter. Fig. 1 illustrates the schematic of the MGC analyzed.

The selected PV plant model is the one described in [13]. The current-voltage (I–V) characteristics of the proposed model were derived using irradiance and temperature as input parameters. The model incorporates a diode, a controlled current source, and two resistances. The operation of the PV power plant is limited by the maximum power point. To improve its efficiency, a boost DC/DC converter is employed to regulate the maximum power point operating strategy (MPPT) utilizing the perturb and observe algorithm. To this end, the duty cycle of the DC/DC converter is employed to adjust the variations in the irradiance to the output power of the PV power plant.

Moreover, a lithium-ion battery energy storage system (BESS) serves as a backup system to the PV solar plant. The selected BESS model is the one developed in [14] and available in the SimPowerSystems toolbox in Simulink.

Finally, each MG is equipped with an RLC filter, an isolation power transformer, and a transmission line, which establishes connections between the individual MGs and the point of common coupling (PCC), while incorporating inductance and loss resistance.

III. Control and Energy Management System

A. Local Control System

This section outlines the control strategy implemented within the MGC, which is structured hierarchically. The local control relies on the droop control method for GFM inverters and on power control for the GFL inverter. The proposed control scheme is depicted in Fig. 2.

The frequency of each MG is described as

$$f_i = f_{o,i} + n_{,i}(P_{o,i} - P_i) \quad (1)$$

where f_i represents the MG frequency, $f_{o,i}$ denotes the reference frequency, n_i is the droop control parameter, $P_{o,i}$ refers to the power at $f_{o,i}$ and P_i indicates the delivered active power.

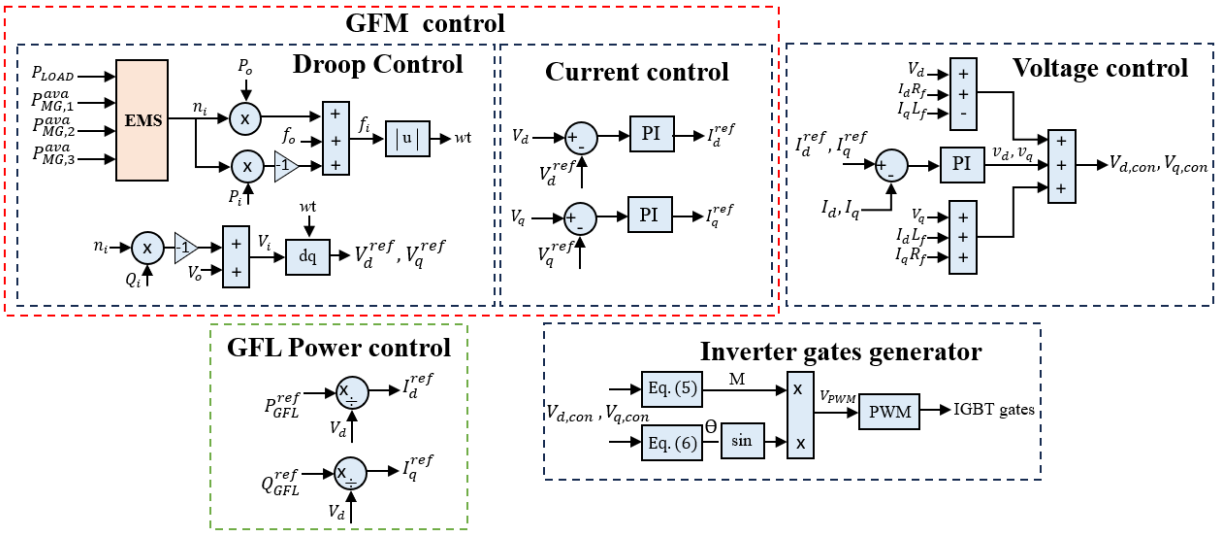

Fig. 2. MGC cascade control scheme.

Analogously, the following equation defines the relationship used to derive the voltage at the MG level:

$$V_i = V_{o,i} - m_i Q_i \tag{2}$$

in Eq. (2), V_i denotes the output voltage, $V_{o,i}$ is the reference voltage, m_i refers to droop voltage coefficient, and Q_i is the injected reactive power. It is important to note that for the voltage droop control, the value of $Q_{o,i}$ is set to zero.

Upon obtaining the value of f_i , the next step is to compute the term wt, that is required to transform the sinusoidal current and voltage measurements (I_{abc}, V_{abc}) into the direct-quadrature reference frame, producing $V_d^*, V_q^*$and I_d^*, I_q^*. This conversion is crucial for the implementation of PI controllers. The subscript "d" denotes the direct component, while "q" represents the quadrature component. Moreover, the superscript "*" indicates the reference values.

The voltage control system is tasked with regulating the measured values of V_d, V_q to match the desired values. This is accomplished through a PI controller that minimizes the error between the actual values of V_d, V_q and their reference values, V_d^*, V_q^*. Consequently, the output of each PI controller generates the reference current values for each converter, denoted as I_d^*, I_q^*.

The target of the current control is to regulate the measured values of I_d, I_q to match the previously determined reference values. A PI controller is employed to match their corresponding reference values, I_d^*, I_q^*. The output signals from these PI controllers, labeled as $v_{d,i}$ and $v_{q,i}$, correspond to the voltage values that each inverter needs to control. Assuming that the 'd' and 'q' components are not entirely independent, it is necessary to isolate the 'd' and 'q' axes. This decoupling is achieved using feedforward decoupling, which calculates the direct and quadrature control components of the inverter ($V_{d,con}, V_{q,con}$) as

$$V_{d,con} = V_d + I_d R_f - I_q L_f + v_{d,i} \tag{3}$$

$$V_{q,con} = V_d + I_d L_f + I_q R_f + v_{q,i} \tag{4}$$

in Eq. (3) and Eq. (4), R_f and L_f refer to the resistance and inductance values associated with the filter.

The generation of pulses for each inverter is carried out by employing a standard pulse width modulation (PWM) technique. The modulation index (M) is calculated based on the expression given in Eq. (5) as

$$M = \left| \frac{V_{d,con}, V_{q,con}}{\frac{V_{DC}}{2} \frac{1}{\frac{V_{sec}^* \sqrt{2}}{\sqrt{3}}}} \right| \tag{5}$$

$$\theta = \angle \left(\frac{V_{d,con}, V_{q,con}}{\frac{V_{DC}}{2} \frac{1}{\frac{V_{sec}^* \sqrt{2}}{\sqrt{3}}}} \right) + wt \tag{6}$$

The control voltage (V_{PWM}) is determined by using the modulation index (M) and the phase angle, as

$$V_{PWM} = M \sin \theta \tag{7}$$

where Θ represents the phase of V_{PWM} , V_{DC} is the input DC voltage, and V_{sec}^* refers to the rated secondary voltage of the power transformer.

The PWM block is tasked with producing the triggering pulses for the IGBTs, regulating both the voltage and frequency in accordance with the delivered power.

For the MG operating with a GFL inverter, the control is based on the reference power that needs to be managed, rather than following the droop control method. To achieve this, a

phase-locked loop (PLL) is initially used to measure the grid voltage V_{abc} and determine the term wt for this MG. The droop control is replaced by a power control, where the reference active power for the MG (P^*_{GFL}) is divided by the measured direct voltage (V_d) to obtain the reference direct current (I^*_d). Similarly, the reference reactive power for the MG (Q^*_{GFL}) is divided by V_d to calculate the reference quadrature current (I^*_q). Once these values are obtained, the remainder of the control process follows the same procedure as for GFM inverters.

The EMS is designed to effectively manage the real-time power distribution among MGs while meeting the system operator's requirements. The proposed EMS is founded on the concept of the real-time available power. The real-time available power in each MG ($P^{ava}_{MG,n}$) is defined by the following expression:

$$P^{ava}_{MG,n} = P_{PV,n} + P_{BESS,n} - P_{LOAD,n} \quad (8)$$

where the term $P_{PV,n}$ refers to the available PV power in each MG, based on the real-time solar irradiance, $P_{BESS,n}$ denotes the power available from the BESS according to its SOC, and $P_{LOAD,n}$represents the local load of each MG.

To constrain the charging and discharging processes of the BESS in each MG, the variation in the SOC at each moment is rigorously accounted for in accordance with:

$$P^{max}_{BESS,dis} = min\left(P^{rated}_{BESS}, \frac{E^{nom}_{BESS}}{\Delta t} \cdot \left(\frac{SOC - SOC_{min}}{100}\right)\right) \quad (9)$$

$$P^{max}_{BESS,ch} = min\left(P^{rated}_{BESS}, \frac{E^{nom}_{BESS}}{\Delta t} \cdot \left(\frac{SOC_{max} - SOC}{100}\right)\right) \quad (10)$$

where $P^{max}_{BESS,dis}$ denotes the maximum power available in discharge mode, and $P^{max}_{BESS,ch}$ represents the maximum power that the BESS can manage in charge mode, the term P^{rated}_{BESS}refers to the rated power of the BESS. $\frac{E^{nom}_{BESS}}{\Delta t}$ represents the rate of change over time of the available energy in the BESS, SOC_{min} is the minimum allowed state of charge in the BESS, and SOC_{max} is the maximum allowed state of charge in the BESS.

As an initial step, a minimum operational power, $P^{res}_{MG,3}$, is assigned to MG_3. Accordingly, the total power that must be distributed between MG_1 and MG_2 (P_{SHARE})is calculated as

$$P_{SHARE} = P^{ref}_{GRID} - P^{res}_{MG,3} \quad (11)$$

where the term P^{ref}_{GRID} represents the reference active power specified by the system operator (SO).

The power distribution between MG_1 and MG_2 is performed proportionally to the real-time available power of each MG. If $P^{ava}_{MG,1} > P^{ava}_{MG,2}$, MG_1 must handle a greater share of the power than MG_2. To achieve this, the droop control coefficient of MG_1 (n_1) should be proportionally smaller than the droop control coefficient of MG_2 (n_2). Conversely, if $P^{ava}_{MG,1} < P^{ava}_{MG,2}$, the power distribution should follow the opposite operation.

Once the droop control coefficients are established, the power injected by each MG is calculated based on these coefficients, resulting in a preliminary distribution of the power to be allocated among the MGs. Subsequently, it is verified whether the preliminary distribution causes any MG to exceed its available power. If $P_{MG,n} > P^{ava}_{MG,n}$, the power output of that MG is limited to $P^{ava}_{MG,n}$, and the power excess—defined as the difference between the preliminarily assigned value and $P^{ava}_{MG,n}$—is managed by MG_3. If the preliminary distribution does not exceed the available capacity of any MG, the initial allocation is selected as the final distribution for each MG.

Finally, the power allocated to MG_3 will be determined as the sum of its minimum reserve power and the surplus power that MG_1 and MG_2 were unable to manage. In the event that MG_3 cannot accommodate this surplus, the MGC is unable to meet the required demand. In such scenario, the maximum manageable power is defined as the sum of the capacities of all MGs.

IV. Results and Discussion

This section presents time-domain simulations performed in MATLAB/Simulink to validate the proposed EMS's effectiveness in managing the power distribution across each MG. This coordination accounts for the intermittency of the PV power plant, variations in the SO demand, and fluctuations in local loads of each MG. The initial is set as follows: SOC_1 at 30%, SOC_2 at 85%, and SOC_3 at 60%.

Fig. 3 illustrates the irradiance profile for the PV power plants in MG_1 (a), MG_2 (b), and MG_3 (c). The SO active power demand is set as follows: 412.5 kW from 0 to 50 s, 300 kW from 50 to 125 s, 600 kW from 125 to 150 s, 525 kW from 150 to 200 s, 187.5 kW from 200 to 225 s, and increases to 468.8 kW in the final segment of the simulation, reaching 250 s.

To satisfy these operational requirements, each MG contributes power in proportion to its instantaneous available capacity. Fig. 4 shows the power delivered by each MG alongside their respective maximum available capacities. To illustrate the allocation process, the first instant of the simulation is considered as an example, where the system operator demands 412.5 kW. In this scenario, MG_1 has a capacity of 180 kW, while MG_2 has a capacity of 337.5 kW. Since the total capacity of both

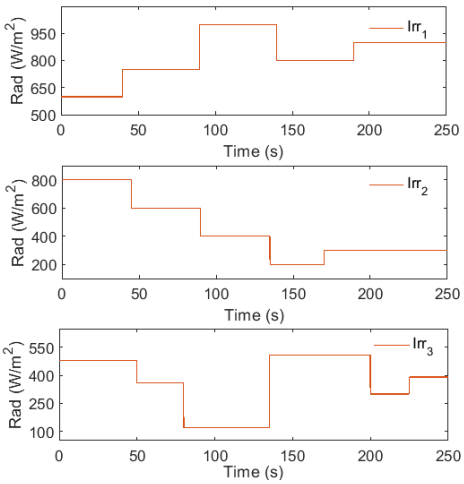

Fig. 3. Radiation profile: (a) MG_1, (b) MG_2 and (a) MG_3.

MGs exceeds the demand, the reserve MG_3 operates at its minimum output level. Given that $P_{MG,1}^{ava}$<$P_{MG,2}^{ava}$, it follows that $P_{MG,1}$ <$P_{MG,2}$to maintain the balance. Consequently, $P_{MG,1}$ is set to 140 kW, $P_{MG,2}$ is set to 262.5 kW, and $P_{MG,3}$ takes the value of 10 kW.

This distribution is maintained and adjusted based on variations in the radiation levels of each PV power plant, the SOC of each BESS, or the requirements of the SO. At the time instant t=150 s, the SO demands 525 kW. With $P_{MG,1}^{ava}$ and $P_{MG,2}^{ava}$ both equal to 220 kW, neither MG has enough capacity to fully meet the demand. Consequently, MG_3 increases its power output to $P_{MG,3}$=85 kW to ensure the balance. When the demand decreases to 187.5 kW at t=200s, the capacities of MG_1 and

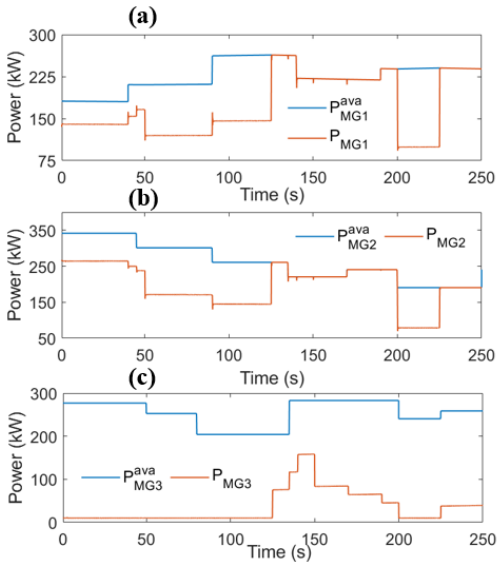

Fig. 4. MG capacity and delivered power: (a) MG1: $P_{MG,1}^{ava}$ and $P_{MG,1}$, (b) MG2: $P_{MG,2}^{ava}$ and $P_{MG,2}$ and (c) MG3: $P_{MG,3}^{ava}$ and $P_{MG,3}$.

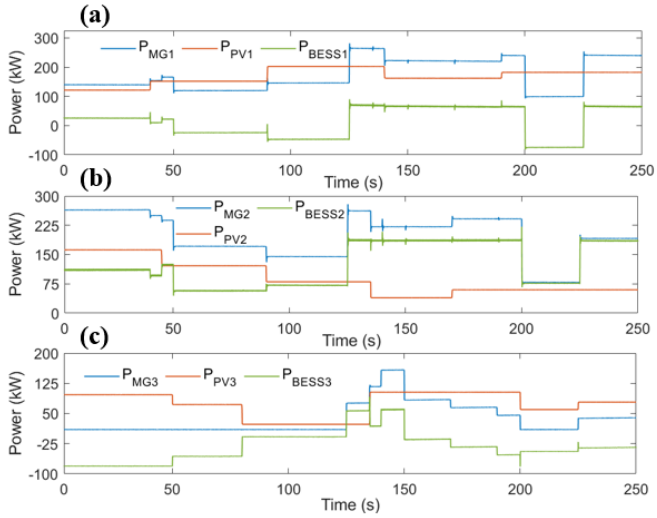

Fig. 5. MG powers: (a) MG1: $P_{MG,1}$, $P_{PV,1}$, $P_{BESS,1}$ (b) MG2: $P_{MG,2}$, $P_{PV,2}$, $P_{BESS,2}$ and (c) MG3: $P_{MG,3}$, $P_{PV,3}$, $P_{BESS,3}$.

MG_2exceed the required value, and MG_3 returns to its minimum operating level of 10 kW.

Fig. 5 presents the values of $P_{MG,n}$,$P_{PV,n}$, and $P_{BESS,n}$. At the initial instant of the simulation, $MG_1$is required to supply 140 kW. With $P_{PV,1}$ providing 121 kW, $BESS_1$ discharges to balance the power, contributing with 19 kW. In the case of MG_2, $P_{PV,2}$ supplies 162.5 kW, with the remaining balance provided by $BESS_2$, delivering a power output of $P_{BESS,2}$ =100 kW. During intervals where $P_{PV,n}$ exceeds the power supplied by each MG, the surplus power is stored in the BESS. For instance, this scenario is observed between 50 s and 125 s for MG_1, where $BESS_1$ receives a charging power ranging from -25 kW to -45 kW.

A notable scenario occurs at t=200s, when a local load of 50 kW is connected to MG_2. As a result, the value of $P_{MG,2}^{ava}$ decreases to 190 kW, with $P_{PV,2}$ at 60 kW and $P_{BESS,2}$ at 75 kW. Therefore, MG_2 is able to meet its local demand of 50 kW while simultaneously supplying 85 kW to the grid, according to the setpoint assigned by the EMS.

Fig. 6 depicts the control of the active power delivered to the grid, where the total power delivered by the MGC (P_{PCC}) consistently matches the SO power reference (P_{GRID}^{ref}). It is demonstrated that the proposed EMS is capable of handling real-time variations in incident radiation, changes in the system operator's demand, and fluctuations in local loads, effectively distributing the power between MGs and ensuring that they do not exceed their available capacities.

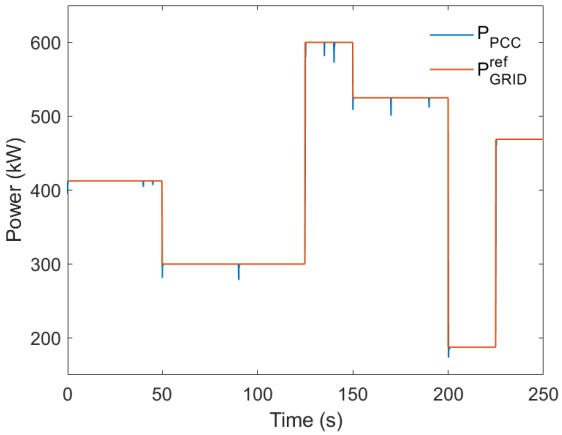

Fig. 6. MGC power control: system operator reference (P_{GRID}^{ref}) and MGC delivered power at PCC (P_{PCC}).

CONCLUSIONS

This paper has presented a dynamic EMS for a MGC composed of MGs operating with GFM and GFL inverters. The concept of real-time available power has been proposed to address the power dispatch between MGs, considering the intermittency of renewable energy sources and demand variability, in contrast to other approaches in the literature that assume ideal generation sources. Based on this concept, it has been validated that the proposed EMS is capable of establishing

an operation that enables proper power distribution between MGs without exceeding their available capacities. Several time-domain simulation scenarios, incorporating intermittency in renewable generation and variability in the system operator's demand, have confirmed the validity of the proposed control approach. Future work will focus on real-word validation and integration of additional renewable energy sources.

REFERENCES

[1] Bandeiras F, Pinheiro E, Gomes M, Coelho P, Fernandes J. Review of the cooperation and operation of microgrid clusters. Renewable and Sustainable Energy Reviews 2020;133. https://doi.org/10.1016/j.rser.2020.110311.

[2] Alam MS, Hossain MA, Shafiullah M, Islam A, Choudhury MSH, Faruque MO, et al. Renewable energy integration with DC microgrids: Challenges and opportunities. Electric Power Systems Research 2024;234. https://doi.org/10.1016/j.epsr.2024.110548.

[3] Bordbari MJ, Nasiri F. Networked Microgrids: A Review on Configuration, Operation, and Control Strategies. Energies (Basel) 2024;17. https://doi.org/10.3390/en17030715.

[4] Liyanage C, Nutkani I, Meegahapola L, Jalili M. Stability Enhancement of Power Synchronisation Control Based Grid-Forming Inverter under Varying Network Characteristics. IEEE Trans Sustain Energy 2024;15:1799–813. https://doi.org/10.1109/TSTE.2024.3379548.

[5] Narendra Babu P. Adaptive grid-connected inverter control schemes for power quality enrichment in microgrid systems: Past, present, and future perspectives. Electric Power Systems Research 2024;230. https://doi.org/10.1016/j.epsr.2024.110288.

[6] Wang X, Wang S, Ren J, Song Z, Zhang S, Feng H. Optimizing Economic Dispatch for Microgrid Clusters Using Improved Grey Wolf Optimization. Electronics (Switzerland) 2024;13. https://doi.org/10.3390/electronics13163139.

[7] Chakraborty A, Ray S. Economic and environmental factors based multi-objective approach for optimizing energy management in a microgrid. Renew Energy 2024;222. https://doi.org/10.1016/j.renene.2023.119920.

[8] Deng F, Zhang L, Xiao Z, Yao Z, Tang Y. Decentralized Multilayer Master-Slave Control Strategy for Power Management in Autonomous DC Microgrid Clusters. IEEE Transactions on Industrial Electronics 2024:1–12. https://doi.org/10.1109/tie.2024.3443949.

[9] Vijay AS, Chandorkar MC, Doolla S. Modified control structures for sharing of asymmetrical powers amongst inverter based distributed energy resources. International Journal of Electrical Power and Energy Systems 2023;152. https://doi.org/10.1016/j.ijepes.2023.109262.

[10] Cosgrove P, Roulstone T, Zachary S. Intermittency and periodicity in net-zero renewable energy systems with storage. Renew Energy 2023;212:299–307. https://doi.org/10.1016/j.renene.2023.04.135.

[11] Z. Wang, L. Guo, X. Li, X. Zhou, J. Zhu and C. Wang, "Multi-Swing PLL Synchronization Transient Stability of Grid-Connected Paralleled Converters," in IEEE Transactions on Sustainable Energy, vol. 16, no. 1, pp. 716-729, Jan. 2025, doi: 10.1109/TSTE.2024.3481417

[12] X. Wu, L. Zhang, Y. Xu, S. Wang and J. M. Guerrero, "Hierarchical and distributed control of AC and DC microgrid clusters interconnected by flexible DC distribution network," in CSEE Journal of Power and Energy Systems, doi: 10.17775/CSEEJPES.2024.01190

[13] The Mathworks. PV power plant. (Online). Accessed:26 March,2025, Available: https://es.mathworks.com/help/sps/ug/detailed-model-of-a-100-kw-grid-connected-pv-array.html

[14] The Mathworks. Battery model. (Online). Accessed:26 March,2025, Available: https://es.mathworks.com/help/sps/powersys/ref/battery.html